Novel topological end modes and breaking of bulk boundary correspondence in skin-effect absent superconductive chain

Huan-Yu Wang (wangjingxiang727@iphy.ac.cn)
Institute of Physics, Chinese Academy of Sciences

Wu-Ming Liu
Institute of Physics, Chinese Academy of Sciences https://orcid.org/0000-0002-1179-2061

Letter

Keywords: Topological nontrivial systems, bulk boundary correspondence, skin effect

Posted Date: October 28th, 2021

DOI: https://doi.org/10.21203/rs.3.rs-1028290/v1

Novel topological end modes and breaking of bulk boundary correspondence in skin-effect absent superconductive chain

Huan-Yu Wang [1*] **and Wu-Ming Liu** [1†]
[1] *Beijing National Laboratory for Condensed Matter Physics, Institute of Physics, Chinese Academy of Sciences, Beijing 100190, China*

Topological nontrivial systems feature isolated gapless edge modes[1–6], and play a key role in advancing our understanding of quantum matter[7–18]. A most profound way to characterize edge modes above is through bulk topological invariants, which is known as bulk boundary correspondence[19–23]. Recent studies on non-Hermitian physics have pronounced the broken bulk-boundary correspondence with the presence of skin effect[24–28]. Here, we propose a new type of fermionic topological edge modes η, satisfying $\eta^\dagger = i\eta, \eta^2 = -i$. Remarkably, we demonstrate that for both two cases: superconductive chain with purely η modes and quantum chain with η, Majorana modes γ on different ends, fermion parity can be well defined. Interestingly, for the latter case, broken bulk boundary correspondence is observed despite the absence of skin effects . The phenomenon above is unique to open quantum systems. For the junction with both η, γ modes, the current will not remain sinusoid form but decay exponentially. The exchange of η modes obeys the rules of non-abelian statistics, and can find its applications in topological quantum computing.

For topological nontrivial Kitaev chain, there can exist unpaired Majorana mode on separated ends, which is also its own antiparticle. Also, Majorana fermions can be viewed as real split part of conventional fermions. Here we split fermion modes in a another way that $c_n = \frac{1}{2}(\eta_{2n} + i\eta_{2n-1}), c_n^\dagger = \frac{1}{2}(\eta_{2n-1} + i\eta_{2n})$. It can be identified that the η modes are fermion modes obeying the anti-commutation rules, however in contrast to Majorana and conventional fermion modes, we have:

$$\eta^\dagger = i\eta, \eta^2 = -i \tag{1}$$

To depict a topological nontrivial chain with isolated η modes on separated end, we consider a one dimensional superconductive chain:

$$H_\eta = -it\sum_{n=1}^{N-1}\eta_{2n}\eta_{2n+1} - \sum_{n=1}^{N}\frac{\mu}{2}\eta_{2n-1}\eta_{2n} \tag{2}$$

where N is the length of the chain and t denotes the tunneling amplitude between adjacent sites. H_η implicates a spin polarized non-Hermitian superconductive chain without skin effect, and the generalized Brillouin zone coincides with the conventional Brillouin zone. Hence, the topological edge modes obtained with open boundary conditions should consist with the bulk topological invariants. The momentum space Hamiltonian of regular fermion presentation reads: $H_\eta(k) = \sum_k d_i(k)\cdot\sigma_i(k)$, with $d_x(k) = -it\sin k$, $d_z(k) = (it\cos k - \frac{\mu}{2})$. For $\mathrm{Re}(\mu) = 0$, we have $H_\eta = iH_0$, and H_0 belongs to BDI class, which can be topologically characterized by the winding number $W = \frac{1}{2\pi}\int_0^{2\pi}[d_x(k)\partial_k d_z(k) - d_z(k)\partial_k d_x(k)]dk$. Topological nontrivial region ($w = -1$) lies in $|\mu| < 2t$.

η, γ modes can be both protected by the presence of symmetry, $\mathcal{U}H(k)\mathcal{U}^{-1} = e^{i\varphi}H(-k)$, and $\mathcal{U}$ is an anti-unitary operator. For example, degenerate Majorana end modes can be regarded as a combination of zero energy state ψ and its symmetric partner state in forms of $\gamma_{0A} = \frac{1}{2}(\psi + \psi^*), \gamma_{0B} = \frac{-i}{2}(\psi - \psi^*)$. Simultaneously, $\eta_{0A} = \frac{1}{2}(\psi - i\psi^*), \eta_{0B} = \frac{1}{2}(\psi^* - i\psi)$ can be obtained. Numerically, η modes can not be differed from Majorana modes by the localization behavior. Hence, to distinguish η and Majorana modes, one has to detect the phase of the modes localized at zero energy. Here, for topological nontrivial zero energy mode τ, we define a phase indicator, $I_\phi = (\tau + \tau^\dagger)^2$, and $I_\phi = 2, 4$ corresponds to η modes, Majorana modes respectively[29].

A superconductive chain with singly isolated η modes on both ends can experience a transition in fermion parity with the boundary conditions changing from periodic to anti-periodic. The Z_2 invariants of the chain with η modes in Eq. (2) are of $Q_\eta = sgn(d_z(k = 0)d_z(k = \pi))$, where topological nontrivial region $Q_\eta = +1$ consists with that obtained via the winding number.

Conventionally, single Majorana mode must coexist with its partner, even though spatially separated. Here we composite an intriguing non-Hermitian quantum chain with combined $\eta - \gamma$ modes (non-partner mode) located at different ends, which is schematically shown in Fig. 1a:

$$H_{\eta-\gamma} = t\sum_{n=0}^{N-1}\eta_{2n}\gamma_{2n+1} + \sum_{n=1}^{N}\frac{\mu}{2}\eta_{2n-1}\eta_{2n} \tag{3}$$

Superconductive quantum chain above also possesses no skin effects with the determinant of transfer matrix being identity. Surprisingly, it is presented that the critical chemical potential where edge modes merge (see Fig. 1b) to the bulk dose not consist with the momentum space gap closing points (see green dashed line in Fig. 1c). The broken bulk-boundary correspondence above is unique to non-Hermitian system of a particular form. In detail, we notice that the quantum chain in momentum space of regular fermion presentation can be read as $H_{\eta-\gamma}(k) = \frac{\lambda t}{2}(\sin k\mathrm{I} - \cos k\sigma_z + \sin k\sigma_x + \sin k\sigma_y) + \frac{\mu}{2}\sigma_z, \lambda = 1 + i$. By restricting $t = t_0\lambda^*$, system above can be of a Hermitian one and there exists no broken bulk boundary

correspondence. Meanwhile, as the $\sin k\mathrm{I}$ term can not generate extra degeneracy, or manipulate the direct band gap amplitude, which denotes the energy difference between the minimum of upper bands above zero energy and the maximum of the lower bands below zero energy. Thus the ignoring of $\sin k\mathrm{I}$ contributes to no differences in topological features, which can be described by the Z_2 index:

$$Q_{\eta-\gamma} = sgn[(\mu - \mathrm{Re}(\lambda t))(\mu + \mathrm{Re}(\lambda t))] \tag{4}$$

However, as we release the limitations on t (generally $t = 1$). The system is purely non-Hermitian, and the edge modes can still hold. Indeed, $\sin k\mathrm{I}$ shifts imaginary and real band gap closing points in a separated way: for eigen-energy $E(k) = \frac{1}{2}(\lambda t \sin k \pm \sqrt{(\mu - \lambda t\cos k)^2 + 2(\lambda t \sin k)^2})$, the gap of real eigen-energy starts to close at $\mu = \pm\mathrm{Re}(\lambda t)$ with critical $k_0 = N\pi, N \in Z$. However the imaginary eigen-energy holds a finite gap $\chi = t$, see Figs. 1d-e, where the gapped the non-Hermitian system can still support edge modes. By further expanding μ, imaginary gap can be closed at $\mu = \pm(\cos k_0' + \sin k_0')t = \pm\sqrt{2}t, k_0' = (2N \pm \frac{1}{4})\pi$. Although the real part of eigen-energy become gapless for the direct gap, but at above critical k_0', an energy difference between upper and lower bands keeps $\chi = \frac{\sqrt{2}t}{2}$, see Figs. 1f-g, which still depicts a gapped region. Hence, according to the gap closing definition in ref[30], we have no topological phase transitions with the varying μ, which is inconsistent with edge modes of open boundary conditions in Fig. 1b. Such inconsistences are indeed caused by the different critical gap closing momentum k_0, k_0' for real and imaginary eigen-energy spectrum, effects of which are unique to non-Hermitian system. Besides, the differences in real-imaginary gap closing critical momentum can physically stem from the shift induced by the $\sin k\mathrm{I}$. Hence, the broken bulk-boundary correspondence can take place in non-Hermitian system of the form $H(k) = \sum_i d_i(k)\cdot\sigma_i, i = 0, 1, 2, 3$. Also, numerical results in Fig. 1c suggest that a consistent bulk boundary correspondence can be retained via the utilization of direct band gaps.

To further illustrate how $d_0(k)\mathrm{I}$ term breaks the bulk boundary correspondence, we notice that there exists arbitrary phase freedom θ in the definition of η modes, which in general can be expressed as, $\eta_{2n} = e^{i\frac{\theta}{2}}c_n - ie^{-i\frac{\theta}{2}}c_n^\dagger, \eta_{2n-1} = e^{-i\frac{\theta}{2}}c_n^\dagger - ie^{i\frac{\theta}{2}}c_n$. Considering above, the quantum chain with purely η modes in phase dependent form can be described as $H_\eta^\theta(k) = (it\cos k - \frac{\mu}{2})\sigma_z + (-it\cos\theta\sin k)\sigma_x + (-it\sin\theta\sin k)\sigma_y$. For $\mathrm{Re}(\mu) = 0$, time reversal symmetry can be preserved regardless of θ, $\Theta H_\eta^\theta(k)\Theta^{-1} = H_\eta^\theta(-k), \Theta = \sigma_x\kappa$, κ is the charge conjugate operator. In non-Hermitian system, time reversal symmetry can also implicate particle hole symmetry, where by denoting $H_\eta^\theta = iH_\eta'$, we have $\Theta H_\eta'(k)\Theta^{-1} = -H_\eta'(-k)$.

Things get a little different for non-Hermitian quantum chain with combined $\eta - \gamma$ mode on different ends,

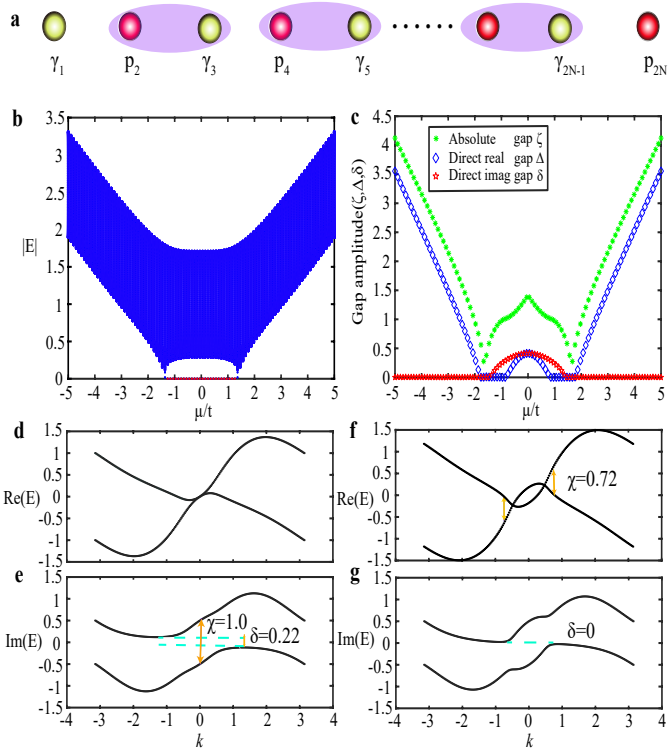

Fig. 1. **a**, A schematic picture of superconductive chain with combined $\eta-\gamma$ modes on different ends. **b**, Eigen-energy spectrum as a function of chemical potential μ in open boundary conditions, and $t = 1$. Blue dashed line depicts the bulk states, and red dashed line depicts the edge modes. **c**, Absolute band gap amplitude ζ in periodical boundary conditions (green dashed lines) varies as a function of μ, which is inconsistent edge modes of open boundary conditions. However, direct real (imaginary) gap amplitude $\Delta(\delta)$ satisfies bulk boundary correspondence respectively. **d-e**, The real part of eigen-energy spectrum has gap closing points at $\mu = \pm 1.0$ with a gapped imaginary eigen-energy spectrum of amplitude $\chi \approx 1.0$. **f-g**, The imaginary part of eigen-energy spectrum has gap closing points at $\mu = \pm 1.42$ with a gapped real energy spectrum of amplitude $\chi \approx 0.72$. Differences in gap closing critical momentum of real and imaginary spectrum result in the broken bulk boundary correspondence.

where there also exists phase gauge freedom for Majorana modes $\gamma_{2n+1} = e^{i\frac{\theta}{2}}c_{n+1} + e^{-i\frac{\theta}{2}}c_{n+1}^\dagger$. The phase dependent Hamiltonian in momentum space reads:

$$\begin{aligned} H_{\eta-\gamma}^\theta =& (-\lambda t(\sin(\theta - k) + \cos(\theta - k)) + \mu)c_k^\dagger c_k \\ &+ (t\sin k)c_k^\dagger c_{-k}^\dagger + (it\sin k)c_{-k}c_k \end{aligned} \tag{5}$$

When we set $\theta_0 = 2N\pi \pm \frac{\pi}{4}, N \in Z$, non-Hermitian Hamiltonian above can be expressed as $H_{\eta-\gamma}^{\theta_0}(k) = d_i(k)\cdot\sigma_i$, where $d_z(k) = -\frac{\sqrt{2}}{2}\lambda t\cos k + \frac{\mu}{2}, d_x = \frac{\lambda t}{2}\sin k, d_y(k) = \frac{\lambda t}{2}\sin k$, and $d_0(k)\mathrm{I}$ terms are absent. Numerical results in Fig. 2a demonstrate a consistent bulk boundary correspondence, and topological nontrivial regions can be depicted by the Z_2 index in Eq.(4). As for general θ, $d_0(k)\mathrm{I}$ terms show up and shift gap closing critical momentum of

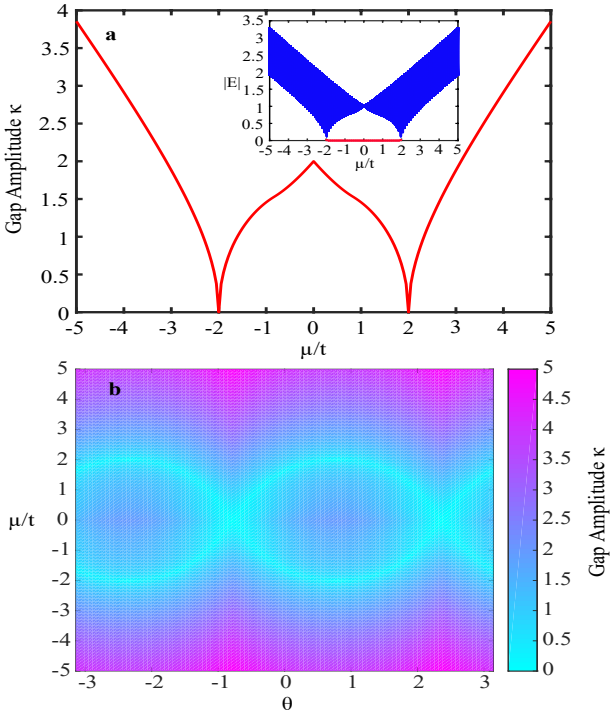

Fig. 2. **a**, The absolute gap amplitude of $H_{\eta-\gamma}$ as a function of chemical potential with $t = 1, \theta = 2N\pi + \frac{\pi}{4}, N \in Z$. The sub-figure shows the corresponding edge modes in open boundary conditions, and conventional bulk boundary correspondence is preserved. **b**, Absolute gap amplitude as a function of chemical potential μ and θ, and bright cyan lines denote gapless region.

real and imaginary spectrum in different ways, breaking the conventional bulk boundary correspondence, which can be inferred from Fig. 2b.

In quantum chain with p-wave pairing, $U(1)$ symmetry is broken and particle number is not an invariant. Hence, system can not remain unchanged under transformation $c'_j = e^{i\phi_0}c_j$ except $\phi_0 = N\pi$, which suggest the topological index Z_2, depicting the fermion parity. Majorana end modes differ from normal fermion modes in that along with a change from periodic to anti-periodic boundary conditions, ground state's fermion parity will get reversed. In the following, we will demonstrate how fermion parity in quantum chain with η modes (or combined $\eta-\gamma$ modes) reacts to changes of boundary conditions.

For a quantum chain with η modes, the coupling between the first and the last site is $H^{\eta}_{boundary} = -it\eta_{2N}\eta_1$, see Fig. 3a. Via defining fermionic operator: $f = \eta_{2N} - i\eta_1$, we have $H^{\eta}_{boundary} = \frac{-it}{2}(f^\dagger f - 2)$, and it can be expressed $H^{\eta}_{boundary} = iH'^{\eta}_0$. Correspondingly, for $t > 0$ in periodic boundary conditions, ground states of H'^{η}_0 is regard as $|\Phi^G_{pbc}\rangle = f^\dagger|0\rangle$. For the anti-periodic boundary conditions ($t < 0$), ground state turns to $|\Phi^G_{apbc}\rangle = f|0\rangle$. A change in fermion parity happens.

For a quantum chain with combined $\eta-\gamma$ modes, the

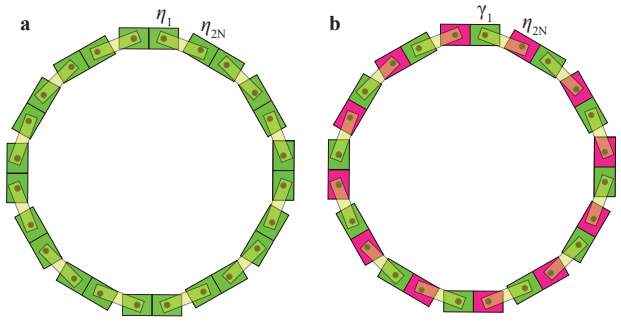

Fig. 3. **a**, In quantum chain of periodic boundary conditions with purely η modes, η_1 and η_{2n} are coupled together. **b**, In quantum chain of periodical boundary conditions with combined $\eta-\gamma$ modes on different ends, γ_1 and η_{2n} are coupled. Changing from periodic to anti-periodic boundary conditions can result in a change of the fermion parity, Q_η and $Q_{\eta-\gamma}$.

coupling between the first and the last site is $H^{\eta-\gamma}_{boundary} = t\eta_{2N}\gamma_1$, see Fig. 3b. Another fermion operator can be defined as $f' = \eta_{2N} - i\gamma_1$, and in this presentation, $H^{\eta-\gamma}_{boundary} = \frac{\lambda t}{2}(f'^\dagger f' - 2)$. In a similar way, by ignoring the imaginary part in coefficient λ, a change from periodic to anti-periodic boundary conditions ($\lambda t \to -\lambda t$) results in a reverse of fermion parity.

As we know, the fractional Josephson effect is closely related to the fermion parity in the junction. Here, for a junction with purely η modes, and $\mathrm{Re}(\mu) = 0$, the system is of pseudo-hermiticity and gain-loss absent. If the junction is wrapped in a head to tail way and in between an insulator barrier is inserted, the current flowing through will be of the sinusoidal form as usual. However, results above are broken for a junction with combined $\eta-\gamma$ modes. To illustrate, we denote states at the left (right) end of the junction to be $\psi_{1(2)}$, and assume $\psi_{1(2)} = \sqrt{n_{1(2)}}e^{i\theta^{1(2)}}$. The two end states are governed by $i\partial_t\psi_{1(2)} = (H^R_{\eta-\gamma} + H^I_{\eta-\gamma})\psi_{1(2)} + K\psi_{2(1)}$, where $H^{R(I)}_{\eta-\gamma} = \frac{1}{2}(H^\dagger_{\eta-\gamma} + (-)H_{\eta-\gamma})$, and K presents the tunneling between two end states of the junction. It can be obtained, in contrast to AC Josephson effect, we have:

$$\frac{1}{2}\partial_t n_{1(2)} = \mathrm{Im}(\mathrm{H}^{\mathrm{I}}_{\eta-\gamma})n_{1(2)} + I_0 \sin(\theta^{2(1)} - \theta^{1(2)}) \qquad (6)$$

where $I_0 = K\sqrt{n_1 n_2}$. Through Eq. (6), the current in combined $\eta-\gamma$ junction will not oscillate in a sinusoidal way, but exponentially decay with time.

It can be shown that the braiding statistics of η modes follow that an exchange of η_n, η_m can be described by the time evolving operator $U = e^{-i\frac{\pi}{4}\eta_n\eta_m}$, of which the non-abelian statistics suggest that η modes can also be utilized as qubits and applied to fault tolerant quantum computing[29]. To achieve a quantum chain of η modes (or combined $\eta-\gamma$ modes) in experiments, we propose to utilize the topolectrical system. A voltage $V(t) = V(0)e^{i\omega t}$ is applied, and the current on each node of the circuit lattice is governed by the Kirchhoff law, $I(\omega) = J(\omega)V(\omega)$, where $J(\omega)$ is the circuit Laplacian. For the

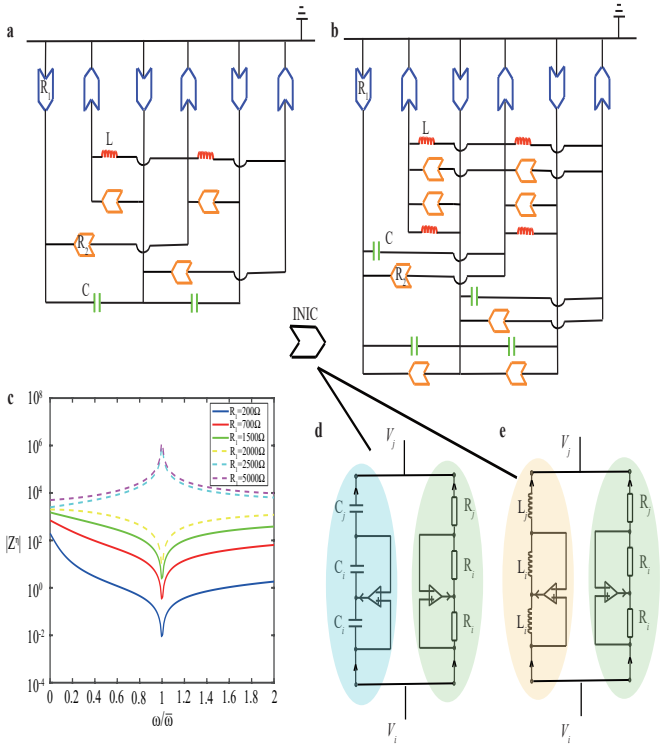

Fig. 4. **a-b**, A circuit lattice realization of a quantum chain with isolated η modes and combined $\eta-\gamma$ modes on different ends. C and L denote the capacitor and inductor respectively. The real part of effective impedance for the blue and orange INICs are R_1 and R_2. **c**, The two point impedance of nodes $1, \mathrm{N}$ for circuit lattice simulating η modes in **a**, $\mathrm{C}=0.25\mu\mathrm{F}, L=10\mu H, R_2=4000\Omega$. The dashed lines highlight topological nontrivial cases for $R_1>2000\Omega$. Boundary resonance are manifested with $\omega=\bar{\omega}$. **d-e**, To simulate the cases when chemical potential is purely real or imaginary, INICs made up of capacitors or inductors shall be applied.

circuit lattice model in Fig. 4a-b, negative impedance converters with current inversion (INICs), of which the impedance can be positive or negative depending on the direction of current, are placed in a staggered way, aiming to simulate the electron and hole bands in the quantum chain. The $J_\eta(\omega), J_{\eta-\gamma}(\omega)$ of the circuit lattices can be expressed as:

$$\frac{J_\eta(\omega)}{i\omega}=\begin{pmatrix} -\frac{2(1-\cos k)}{\omega^2 L}-\frac{1}{i\omega R_1} & -2\frac{\sin k}{\omega R_2} \\ -2\frac{\sin k}{\omega R_2} & 2C(1-\cos k)+\frac{1}{i\omega R_1}\end{pmatrix}$$
$$\frac{J_{\eta-\gamma}(\omega)}{i\omega}=\begin{pmatrix} -\frac{2(1-\cos k)}{\omega^2 L}-\frac{1}{i\omega R_1}-\frac{2\sin k}{\omega R_2} & -2\frac{\sin k}{\omega R_2}+\frac{e^{ik}}{\omega^2 L}-Ce^{-ik} \\ -2\frac{\sin k}{\omega R_2}-Ce^{ik}+\frac{e^{-ik}}{\omega^2 L} & 2C(1-\cos k)+\frac{1}{i\omega R_1}-\frac{2\sin k}{\omega R_2}\end{pmatrix} \quad (7)$$

where $\frac{1}{i\omega C}$, $i\omega L$ and $R_{1(2)}$ are the impendence of the capacitor, inductor and the INICs. By setting the resonant frequency $\omega=\frac{1}{\sqrt{LC}}$, we shall have J_η be capable of simulating $H_\eta(k)$ with $\frac{t}{2}=\frac{1}{\bar{\omega}L}=\bar{\omega}C=\frac{1}{R_2}$ and $\mu=2(it+\frac{1}{R_1})$.

To detect the nontrivial η edge modes via topolectrical circuits, we concentrate on the two point impedance of the nodes pinned at the left and right ends of the circuit lattice in Fig. 4a, $Z^\eta=G(1,N)+G(N,1)-G(1,1)-G(N,N)$, and $G=J^{-1}$. In Fig. 4c, two point impedance $|Z^\eta|$ is most manifested for the resonant frequency $\omega=\bar{\omega}=\sqrt{\frac{1}{LC}}$, and for $R_1>\frac{R_2}{2}$, the peaks of $|Z^\eta|$ describe the topological nontrivial region with isolated η modes at both ends.

Our results have guided us to a further profound understanding of topological physics in open quantum system: unique to non-Hermitian system of the form $H=\sum_i d_i\cdot\sigma_i, i=0,1,2,3$, bulk-boundary correspondence can be broken despite the absence of skin effects. Although fermion parity in quantum chains (junctions) can still be well defined, the current flowing through is not guaranteed to be of the AC sinusoidal form, and can also decay exponentially, also in which system initial quantum phase can be memorized. Reversely, phenomenon above can be utilized to set up phase-detecting quantum devices. For the future research, we suggest to concentrate other quantum structures where η modes can lie, and how it melts in the conditions of finite temperature. Our works also pave the way for searching new type of topological edge modes, which can serves as qubits in fault tolerant quantum computing.

References

[1] Kitaev, A. Y. Unpaired majorana fermions in quantum wires. *Phys.-Usp.* **44**, 131 (2001).

[2] Wang, H.-Y., Znuan, L., Gao, X.-L., Zhao, X.-D. & Liu, W.-M. Robust majorana edge modes with low frequency multiple time periodic driving. *J. Phys.: Condens. Matter.* **32**, 355404 (2020).

[3] Jiang, L. *et al.* Majorana fermions in equilibrium and in driven cold-atom quantum wires. *Phys. Rev. Lett.* **106**, 220402 (2011).

[4] Alicea, J. New directions in the pursuit of majorana fermions in solid state systems. *Rep. Prog. Phys.* **75**, 076501 (2012).

[5] Meier, E. J., An, F. A. & Gadway, B. Observation of the topological soliton state in the su-schrieffer-heeger model. *Nat. Commun.* **7**, 13986 (2016).

[6] Obana, D., Liu, F. & Wakabayashi, K. Topological edge states in the su-schrieffer-heeger model. *Phys. Rev. B* **100**, 075437 (2019).

[7] Wang, H.-Y. *et al.* Topological supersolidity of dipolar fermi gases in a spin-dependent optical lattice. *J. Phys.: Condens. Matter.* **32**, 235701 (2020).

[8] Qi, X.-L. & Zhang, S.-C. Topological insulators and superconductors. *Rev. Mod. Phys.* **83**, 1057–1110 (2011).

[9] Qi, X.-L., Hughes, T. L. & Zhang, S.-C. Topological field theory of time-reversal invariant insulators. *Phys. Rev. B* **78**, 195424 (2008).

[10] Keleş, A., Zhao, E. & Liu, W. V. Effective theory of interacting fermions in shaken square optical lattices. *Phys. Rev. A* **95**, 063619 (2017).

[11] Zeng, Q.-B. & Xu, Y. Winding numbers and generalized mobility edges in non-hermitian systems. *Phys. Rev. Research* **2**, 033052 (2020).

[12] Zhao, E. Topological circuits of inductors and capacitors. *Annals of Physics* **399**, 289 (2018).

[13] Hofmann, T., Helbig, T., Lee, C. H., Greiter, M. &

Thomale, R. Chiral voltage propagation and calibration in a topolectrical chern circuit. *Phys. Rev. Lett.* **122**, 247702 (2019).
[14] Wang, C. & Levin, M. Topological invariants for gauge theories and symmetry-protected topological phases. *Phys. Rev. B* **91**, 165119 (2015).
[15] Gong, M., Tewari, S. & Zhang, C. Bcs-bec crossover and topological phase transition in 3d spin-orbit coupled degenerate fermi gases. *Phys. Rev. Lett.* **107**, 195303 (2011).
[16] Kawabata, K., Higashikawa, S., Gong, Z., Ashida, Y. & Ueda, M. Topological unification of time-reversal and particle-hole symmetries in non-hermitian physics. *Nat. Commun.* **10**, 297 (2019).
[17] Ezawa, M. Braiding of majorana-like corner states in electric circuits and its non-hermitian generalization. *Phys. Rev. B* **100**, 045407 (2019).
[18] Li, L., Lee, C. H., Mu, S. & Gong, J. Critical non-hermitian skin effect. *Nat. Commun.* **11**, 5491 (2020).
[19] Xiao, L. *et al.* Non-hermitian bulk-boundary correspondence in quantum dynamics. *Nat. Phys.* **16**, 761 (2020).
[20] Edvardsson, E., Kunst, F. K. & Bergholtz, E. J. Non-hermitian extensions of higher-order topological phases and their biorthogonal bulk-boundary correspondence. *Phys. Rev. B* **99**, 081302 (2019).
[21] Yang, Z., Zhang, K., Fang, C. & Hu, J. Non-hermitian bulk-boundary correspondence and auxiliary generalized brillouin zone theory. *Phys. Rev. Lett.* **125**, 226402 (2020).
[22] Imura, K.-I. & Takane, Y. Generalized bulk-edge correspondence for non-hermitian topological systems. *Phys. Rev. B* **100**, 165430 (2019).
[23] Wang, X.-R., Guo, C.-X. & Kou, S.-P. Defective edge states and number-anomalous bulk-boundary correspondence in non-hermitian topological systems. *Phys. Rev. B* **101**, 121116 (2020).
[24] Kunst, F. K., Edvardsson, E., Budich, J. C. & Bergholtz, E. J. Biorthogonal bulk-boundary correspondence in non-hermitian systems. *Phys. Rev. Lett.* **121**, 026808 (2018).
[25] Yao, S. & Wang, Z. Edge states and topological invariants of non-hermitian systems. *Phys. Rev. Lett.* **121**, 086803 (2018).
[26] Yokomizo, K. & Murakami, S. Non-bloch band theory of non-hermitian systems. *Phys. Rev. Lett.* **123**, 066404 (2019).
[27] Borgnia, D. S., Kruchkov, A. J. & Slager, R.-J. Non-hermitian boundary modes and topology. *Phys. Rev. Lett.* **124**, 056802 (2020).
[28] Okuma, N., Kawabata, K., Shiozaki, K. & Sato, M. Topological origin of non-hermitian skin effects. *Phys. Rev. Lett.* **124**, 086801 (2020).
[29] See supplementary materials for details on: the localization behavior of quantum chain with isolated η modes; how I_ϕ differentiate isolated η modes, majorana modes; physical effects of $\sin \mathrm{k}\mathrm{I}$ term .
[30] Shen, H., Zhen, B. & Fu, L. Topological band theory for non-hermitian hamiltonians. *Phys. Rev. Lett.* **120**, 146402 (2018).

Methods

Absence of skin effects in superconductive chain with η modes and combined $\eta-\gamma$ modes. The absence of skin effects can be illustrated via a transfer matrix approach. In detail, given Nambu basis $\phi_n = (c_n, c_n^\dagger)^{\mathrm{T}}$, the Hamiltonian H_η can be restated as:

$$H_\eta^{Nambu} = \phi_n^\dagger J_1 \phi_{n+1} + \phi_{n+1}^\dagger J_2 \phi_n + \phi_n^\dagger J_3 \phi_n \quad (8)$$

and the transfer matrix can be obtained as $T_\eta = \begin{pmatrix} J_1^{-1}(\epsilon\mathbf{I}-\frac{\mu}{2}\sigma_z) & -J_1^{-1}J_2 \\ \mathbf{I} & 0 \end{pmatrix}$, where $J_1 = \begin{pmatrix} \frac{i}{2} & -1 \\ 0 & -\frac{i}{2} \end{pmatrix}, J_2 = \begin{pmatrix} \frac{i}{2} & 0 \\ 1 & -\frac{i}{2} \end{pmatrix}, J_3 = \begin{pmatrix} \frac{-\mu}{2} & 0 \\ 0 & \frac{\mu}{2} \end{pmatrix}$. Hence, we have $\det(T_\eta) = 1$, which indicates that as the wave packet propagates, it remain its norm, and there exists no skin effect. Also, the absence of skin effect in combined $\eta-\gamma$ chain can be derived in a similar way. $H_{\eta-\gamma}^{Nambu} = \phi_n^\dagger J_1' \phi_{n+1} + \phi_{n+1}^\dagger J_2' \phi_n + \phi_n^\dagger J_3' \phi_n$, and $J_1' = \begin{pmatrix} -\frac{i}{2} & -i \\ 0 & \frac{1}{2} \end{pmatrix}, J_2' = \begin{pmatrix} -\frac{1}{2} & 0 \\ -1 & \frac{i}{2} \end{pmatrix}, J_3' = \begin{pmatrix} \frac{\mu}{2} & 0 \\ 0 & -\frac{\mu}{2} \end{pmatrix}$. $\det(T_{\eta-\gamma}) = -J_1^{-1}J_2 = 1$, which indicates the absence of skin effect.

Braiding statistics of η modes and application to topological quantum computing. The exchange of η modes are governed by the non-abelian braiding statistics. To show that explicitly, we present the fermion parity on ith site as:

$$P_i^R = 1 - \eta_{2i-1}\eta_{2i} \quad (9)$$

$P_i^R|...0(i)..\rangle = |...0(i)..\rangle$, $P_i^R|...1(i)..\rangle = -|...1(i)..\rangle$. The total fermion parity can be of the form:

$$P_{tot}^R = \prod_i P_i^R \quad (10)$$

Upon exchanging η_n, η_m mode in a T junction via U_{nm}, fermion parity is preserved, $[U_{nm}, P_{tot}^R] = 0$. Considering all above, we can express the exchanging operator as:

$$U_{nm} = e^{-i\beta\eta_n\eta_m} = \cos\beta - i\sin\beta\eta_n\eta_m \quad (11)$$

where β is a real constant and $(\eta_n\eta_m)^2 = 1$. Upon the exchanging process, we have:

$$\begin{aligned} \eta_m &= U_{nm}\eta_n U_{nm}^\dagger = \cos 2\beta\eta_n + \sin 2\beta\eta_m \\ \eta_n &= U_{nm}\eta_m U_{nm}^\dagger = \cos 2\beta\eta_m - \sin 2\beta\eta_n \end{aligned} \quad (12)$$

It can be seen that $\beta = \frac{\pm\pi}{4}$ fulfill the exchanging formalism, and $U_{nm} = e^{-i\pm\frac{\pi}{4}\eta_n\eta_m}$. The non-abelian braiding statistics imply the applications in fault tolerant quantum computing.

Acknowledgements
We are really grateful to Yong Xu, Lin-hu Li, Qi-Bo Zeng, Ronny Thomale, Ru-Quan Wang for helpful discussion. This work was supported by the National Key R and D Program of China under grants No. 2016YFA0301500, NSFC under grants Nos. 61835013.

Author contributions
Huan-Yu Wang planned the work and carried out the numerics. Huan-Yu Wang wrote the manuscript. Wu-Ming Liu supervised the work.

Corresponding author:
∗ wangjingxiang727@iphy.ac.cn
† wliu@iphy.ac.cn

Supplementary Files

This is a list of supplementary files associated with this preprint. Click to download.

- huanyu2suppl.pdf